The Vorticity Balance in the Tropical Upper Troposphere of a General Circulation Model

PRASHANT D. SARDESHMUKH[1]

Geophysical Fluid Dynamics Program, Princeton University, Princeton, NJ 08540

ISAAC M. HELD

Geophysical Fluid Dynamics Laboratory/NOAA, Princeton University, Princeton, NJ 08540

(Manuscript received 11 April 1983, in final form 15 November 1983)

ABSTRACT

The time mean vorticity balance in the summertime tropical upper troposphere of an atmospheric general circulation model constructed at the Geophysical Fluid Dynamics Laboratory is examined, with particular emphasis on the detailed balance in the Tibetan anticyclone. The model produces a reasonable simulation of the large-scale features of the northern summer 200 mb flow in the tropics, without the inclusion of subgrid scale processes that strongly damp the upper tropospheric vorticity. The vorticity balance is essentially nonlinear and nearly inviscid. There is considerable cancellation between the stretching and horizontal advection of vorticity by the time mean flow in the vicinity of the Tibetan anticyclone, with much of the remainder balanced by vertical advection and twisting. Mixing by the resolved transients is not negligible in some regions, but considerably smaller than the horizontal advection overall and less well correlated with the stretching. Subgrid scale mixing (consisting only of a biharmonic horizontal diffusion) plays a negligible role in this vorticity budget.

To relate this study to linear models of the stationary flow in the tropics, the steady state barotropic vorticity equation on the sphere is linearized about the GCM's July mean zonal flow at 200 mb and forced with the GCM's July mean vortex stretching. It is found that the strength of the Tibetan anticyclone can be reproduced only by including a very strong damping of vorticity in this linear model. The strong damping needed by other authors (e.g., Holton and Colton) in their linear diagnoses of the tropical upper tropospheric vorticity balance is therefore interpreted as possibly accounting for neglected nonlinearities, and not necessarily cumulus friction. Our conclusions are, however, potentially suspect, since the terms in our vorticity budget have considerable structure on the smallest scales that can be resolved by the GCM.

1. Introduction

Krishnamurti's (1971a) analyses of the observed 200 mb tropical flow field during the Northern Hemisphere summer for 1967 suggest that the seasonal mean vorticity attains its minimum values near where the divergence attains its maximum values, and vice versa. Such a phase relationship has immediate implications for tropical dynamics, as pointed out by Holton and Colton (1972). Ignoring the vertical advection and twisting terms, the pressure-coordinate vorticity equation at 200 mb can be written

$$0 \approx \frac{\partial \zeta}{\partial t} \approx -\mathbf{V}\cdot\nabla\zeta - \beta v - (f+\zeta)\nabla\cdot\mathbf{V} + F. \quad (1)$$

Here ζ and $\mathbf{V}$ refer to the seasonal mean vorticity and horizontal velocity, while F represents the effects of both large and small scale transients. At the point where ζ is a minimum, $\mathbf{V}\cdot\nabla\zeta = 0$. If $\nabla\cdot\mathbf{V}$ is a maximum near this point, $\mathbf{V}\cdot\nabla\zeta$ clearly cannot balance the vortex tube stretching, $-(f+\zeta)\nabla\cdot\mathbf{V}$, as $f+\zeta$ is observed to be nonzero. Further, one expects βv to be small at the vorticity center as long as the streamfunction ψ ($\zeta = \nabla^2\psi$, $v \approx \partial\psi/\partial x$) and ζ are basically 180 deg out of phase. The only remaining possibility in (1) is that F balances the stretching.

Holton and Colton support this argument by solving the steady state barotropic vorticity equation linearized about the observed zonal mean flow and forced with stretching, computed from Krishnamurti's analysis. They find that the observed streamfunction at 200 mb, the Tibetan anticyclone in particular, can be reproduced only by including a strong damping of vorticity in the model. They obtain a realistic streamfunction by setting $F = -D\zeta$ with $1/D \approx 0.7$ days. Weaker damping yields streamfunction fields with much too large amplitudes and incorrect phases. A number of other authors have used strong damping of momentum or vorticity in linear models of monsoonal and Walker circulations (Chang, 1977a; Gill, 1980). Others (Colton,

[1] Current affiliation: U.K. Atmospheric Modelling Group, Department of Meteorology, University of Reading, Reading, England.

1973; Abbott, 1977; see Chang, 1977b for a review) have attempted to include nonlinear effects in their models to see if nonlinearity can somehow account for at least part of the required "dissipation," and have generally concluded that indeed it can. However, strong dissipation is still needed for consistency of the observed flow, particularly the relative phase of the streamfunction and velocity potential. Whether or not this requirement is simply a consequence of other deficiencies in these models is unclear. A hint that this is the case is provided by Kanamitsu (1977), who obtains a reasonable position of the Tibetan high without strong damping in a model which differs in a number of ways from Abbott's, the most important of which (the author speculates) is the inclusion of the advection of relative vorticity by the divergent part of the flow.

Holton and Colton proposed two possible mechanisms for the apparent strong vorticity damping in the tropical upper troposphere: transients that result in the vorticity and divergence being negatively correlated in time, so that the magnitude of time-averaged stretching $-(f+\zeta)\nabla\cdot\mathbf{V}$ is seriously overestimated if computed with the time-mean fields, and transport by cumulus convection. This latter effect has been proposed to account for the residuals in numerous vorticity budget studies on smaller scales made over the tropical western Pacific (Williams and Gray, 1973; Reed and Johnson, 1974; Hodur and Fein, 1977; Chu *et al.*, 1981) and eastern Atlantic (Shapiro, 1978; Stevens, 1979; Reeves *et al.*, 1979). A tendency can be discerned in these studies for the residual in the vorticity equation, or apparent vorticity source, to be negative in the lower and positive in the upper troposphere; this is generally attributed to the effects of cumulus convection. A similar diagnostic study of the large-scale upper tropospheric vorticity budget over the entire tropics has been attempted by Fein (1977) using Krishnamurti's analyses. Fein's residuals are of the same order of magnitude as those required by Holton and Colton, but they are just as large in the midocean troughs (where one expects little deep convection) as in the Tibetan anticyclone, and have no well-defined sign.

Note that if one accepts the assertion that cumulus-scale transports play a dominant role in the vorticity budget, one is led to conclude that general circulation models in which there is no explicit momentum transport in the cumulus parameterization are incapable of simulating a feature of the monsoonal circulation as basic as the location of the Tibetan high. It is this observation that has motivated the present work.

In this paper we describe the time-mean vorticity budget of a spectral general circulation model constructed at the Geophysical Fluid Dynamics Laboratory (GFDL). There is no explicit momentum transfer in the model's cumulus parameterization, and yet the model does reproduce many features of the Asian monsoonal circulation. A description of the model and its performance at several different resolutions can be found in Manabe *et al.*, (1979). The version analyzed here has the highest resolution of the models described by Manabe *et al.*, namely, rhomboidal truncation at zonal wavenumber 30.

We examine one July simulation and perform the vorticity budget analysis at the 0.205 sigma-coordinate surface. Since the vorticity equation in sigma-coordinates is one of the spectral model's prognostic equations, we obtain an exactly balanced vorticity budget by taking care to evaluate all terms precisely as in the model.

We find that the model's vorticity balance is essentially nonlinear and nearly inviscid. Transience plays only a modest role, and the sub-grid scale mixing (consisting only of a biharmonic horizontal diffusion) is of even less importance. Furthermore, when we linearize the steady-state barotropic vorticity equation about the model's July mean zonal flow at 200 mb and force it with the model's July mean stretching, $-(f+\zeta)\nabla\cdot V$, the conclusion we reach is similar to that of Holton and Colton; the model's streamfunction can be approximately reproduced only if a very strong damping of vorticity is included. However, in this case the large damping is crudely accounting for nonlinearity in the horizontal advection, and, to a lesser extent, vertical advection and twisting, and not cumulus transport of momentum nor, to a first approximation large-scale transients.

A brief description of the model and some pertinent aspects of its simulation of the July tropical circulation is provided in Section 2. In Section 3 the relationships between terms in the sigma- and pressure-coordinate vorticity equations are discussed. The model's vorticity budget is described in Section 4, and calculations with the linearized barotropic vorticity equation in Section 5.

2. The model and its July climatology

The primitive equation model utilized is finite differenced in the vertical using $\sigma = p/p_s$ as the vertical coordinate, where p is pressure and p_s is surface pressure. The prognostic variables are relative vorticity, divergence, temperature, and water vapour mixing ratio (defined on the σ = 0.025, 0.095, 0.205, 0.350, 0.515, 0.680, 0.830, 0.940, and 0.990 surfaces), and the logarithm of surface pressure. All fields are decomposed into spherical harmonics for computation of horizontal derivatives, but transformed back to grid points for the computation of nonlinear products, radiative heating, boundary layer fluxes and convective adjustment. This transform grid has 80 Gaussian latitude points from pole to pole and 96 regularly spaced points on each latitude circle. The model's topography is obtained by decomposing the earth's topography into spherical harmonics and truncating just as for the flow field—with rhomboidal truncation at zonal wavenumber 30. The resulting topography of the Tibetan plateau is displayed in Fig. 1.

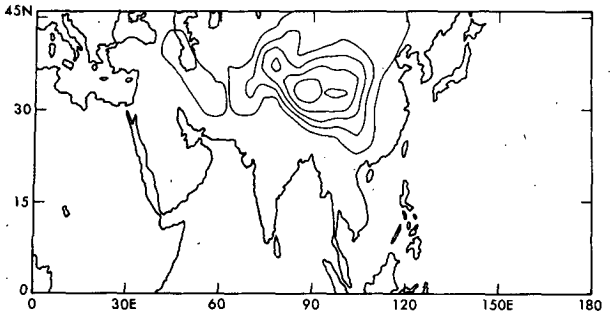

FIG. 1. Topography of the Tibetan plateau. Contour interval is 1 km.

A description of the physical processes included in the model can be found in Manabe *et al.* (1979). Cloud cover is prescribed and is uniform in time and longitude. The seasonal variation of sea surface temperatures is also prescribed, while surface temperatures over continents are determined by the condition that no heat is stored in the soil. Most importantly, the model's treatment of the hydrologic cycle includes, as its parameterization of moist convection, the "moist convective adjustment" proposed by Manabe *et al.* (1965), which redistributes heat and moisture in the vertical but does not redistribute horizontal momentum.

The time integration is semi-implicit with a Robert filter for damping very high frequency variations. Initial conditions for the July simulation are taken from the 30 May results of a lower resolution spectral model.

Figure 2 shows the July mean streamfunction ψ_σ and velocity potential χ_σ on the $\sigma = 0.205$ surface. The time-mean horizontal velocity field is determined by ψ_σ and χ_σ through the relation

$$\mathbf{V} = \mathbf{k} \times \nabla_\sigma \psi_\sigma + \nabla_\sigma \chi_\sigma, \tag{2}$$

where the subscript σ on the gradient operator indicates that the differentiation is performed at constant σ. Fig. 3 shows the corresponding σ-coordinate vorticity, $\zeta_\sigma = \nabla_\sigma^2 \psi_\sigma$, and divergence, $D_\sigma = \nabla_\sigma^2 \chi_\sigma$. Since there is considerable small scale structure in the time mean ζ_σ and D_σ fields, for clarity we show only the Eastern Hemisphere between the equator and 45°N.

Before discussing these fields, we note that the pressure-coordinate vorticity ζ and divergence D are related to ζ_σ and D_σ by

$$\left.\begin{aligned} \zeta &= \zeta_\sigma + \mathbf{k} \cdot \left[\frac{\partial \mathbf{V}}{\partial \ln \sigma} \times \nabla \ln p_s \right] \\ D &= D_\sigma - \frac{\partial \mathbf{V}}{\partial \ln \sigma} \cdot \nabla \ln p_s \end{aligned}\right\}. \tag{3}$$

Computing the corrections $\zeta - \zeta_\sigma$ and $D - D_\sigma$ each time step and then averaging in time at $\sigma = 0.205$, we obtain the ζ and D fields shown in Fig. 4. The differences between (ζ, D) and (ζ_σ, D_σ) are significant near large topographic slopes, but these differences do not change the qualitative structure of the fields. Interpolating ζ and D to a constant pressure surface (200 mb, say) introduces additional modifications comparable in magnitude to the difference between Figs. 3 and 4. (The difference between averaging in time at constant σ and then interpolating to 200 mb using the time mean p_s, rather than interpolating to 200 mb each time step and then time averaging, is negligible.)

Because of the small scales of the topographic slopes, the differences between (ψ, χ) and $(\psi_\sigma, \chi_\sigma)$ are even less pronounced than the differences in vorticity and divergence, and plots of ψ and χ are very similar to those in Fig. 2.

The model's streamfunction bears a close resemblance in the Asian monsoonal region to that obtained by Krishnamurti (1971b; his Fig. 2). The anticyclone is centered close to the Tibetan plateau, while the anticyclonic circulation in the southern Indian ocean is split into two centers, one north of Australia and another in the central Indian ocean. In contrast, the velocity potential differs markedly from Krishnamurti's; the latter has a minimum on the west coast of the bay of Bengal, while Fig. 2 shows an elongated minimum extending from north of the Phillipines to the equator

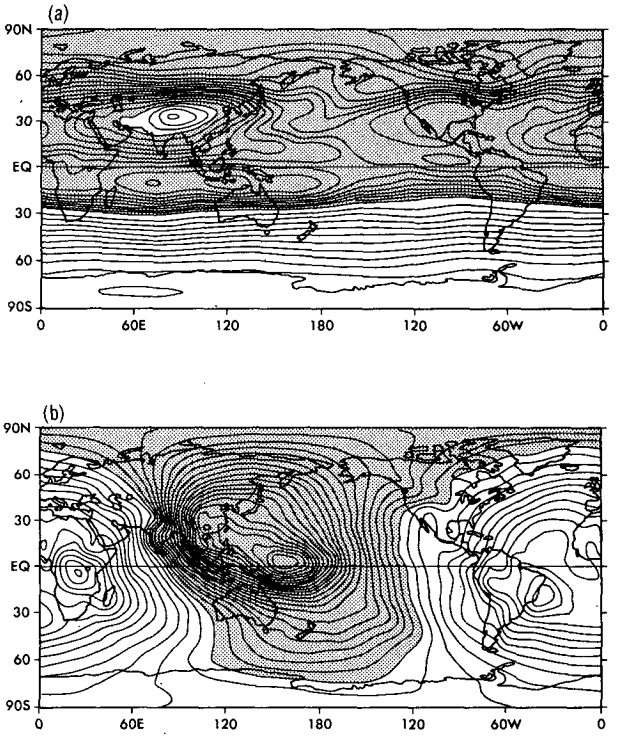

FIG. 2. (a) July mean streamfunction ψ_σ at $\sigma = 0.205$ as simulated in the model. Negative values are shaded. Contour interval is 5×10^6 m^2 s^{-1} except in the Southern Hemisphere where positive values occurring south of ~30°S are contoured with an interval of 15×10^6 m^2 s^{-1}. (b) Velocity potential x_σ at $\sigma = 0.205$. Negative values are shaded. Contour interval is 10^6 m^2 s^{-1}.

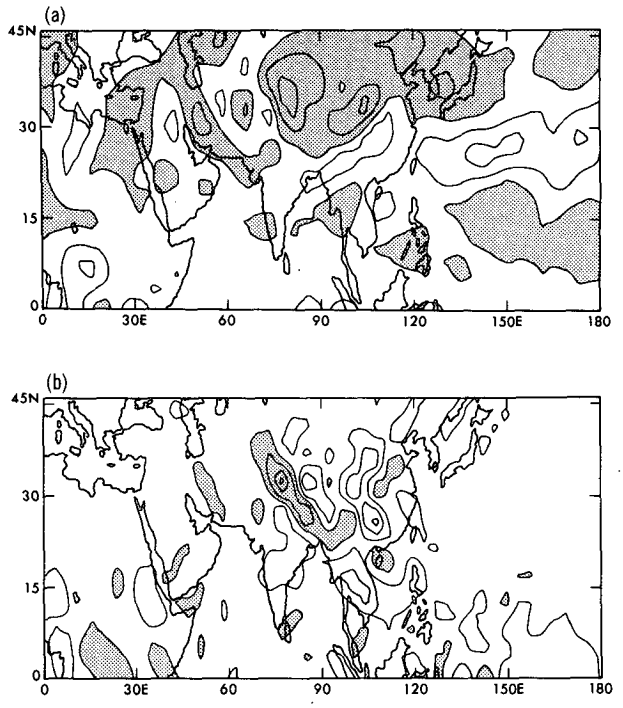

FIG. 3. (a) July mean σ-coordinate vorticity ζ_σ. Contour interval is 2×10^{-5} s^{-1}; the contour lines corresponding to $\pm 1, \pm 3, \pm 5 \times 10^{-5}$ s^{-1} are drawn. Values less than -1×10^{-5} s^{-1} are shaded. (b) Divergence D_σ at $\sigma = 0.205$. Contour interval is 10^{-5} s^{-1}. Contour lines corresponding to $\pm 0.5, \pm 1.5, \pm 2.5, \pm 3.5 \times 10^{-5}$ s^{-1} are drawn. Values less than -0.5×10^{-5} s^{-1} are shaded.

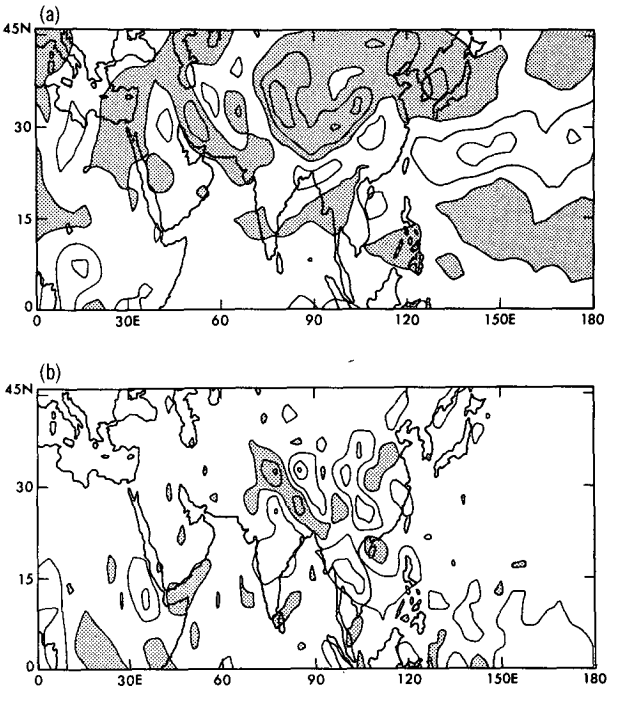

FIG. 4. As in Fig. 3 except for (a) the pressure coordinate vorticity ζ, and (b) divergence D.

at ~160°E. An analysis of FGGE data for 16–30 June 1979 (Bengtsson *et al.*; 1982) yields a velocity potential that resembles Fig. 2 somewhat more closely: the minimum appears over the Phillipines, with low values penetrating southeastwards. The velocity potential in the monsoon region obtained from this FGGE analysis thus falls roughly halfway between Krishnamurti's analysis for 1967 and Fig. 2.

There is substantial spatial separation in the model between the minimum in χ and the maximum in ψ; in fact the maximum in ψ falls near the zero-line in χ. (A similar relationship occurs in the FGGE data referred to before since the center of the anticyclone in that data set occurs over Afghanistan rather than Tibet). But we emphasize that this phase relationship has little direct relevance to the vorticity balance since considerably smaller scales in the flow dominate the vorticity and divergence (Figs. 3 and 4). The vorticity bears no simple relationship to the divergence, although there is a hint of a 90° phase difference that becomes more obvious from the plot of vorticity advection in Section 4.

A striking feature in D and D_σ is the strong convergence south of the Tibetan plateau, more or less paralleling the Ganges river valley, and contrasting with the divergence over the rest of the continental area. The corresponding downward motion is reflected in the July-mean precipitation pattern produced by the model, shown in Fig. 5. A dry belt south of the Tibetan plateau is also found in observations, as indicated in Fig. 6, redrawn from the monograph of Rao (1976). This belt lies between the path of monsoon depressions to the south and the rainfall in the mountains to the north. The model's dry belt is much more intense than that in Fig. 6, and extends too far towards the Bay of Bengal, but its position is basically correct. The model does produce synoptic-scale disturbances that bear at least a superficial resemblance to monsoon depressions, as described in Sardeshmukh (1982).

Further information on the model's July-mean fields of surface pressure and precipitation, zonal mean

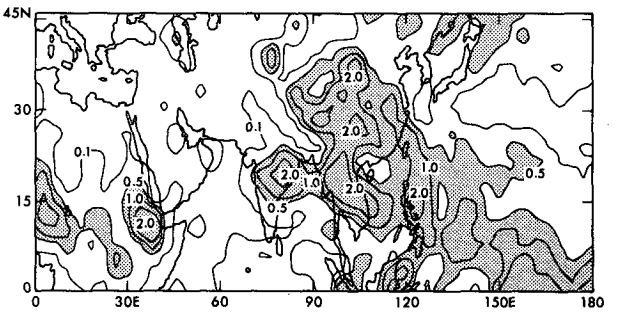

FIG. 5. July mean precipitation. The contours are 0.1, 0.5, 1.0, and 2.0 cm day^{-1}.

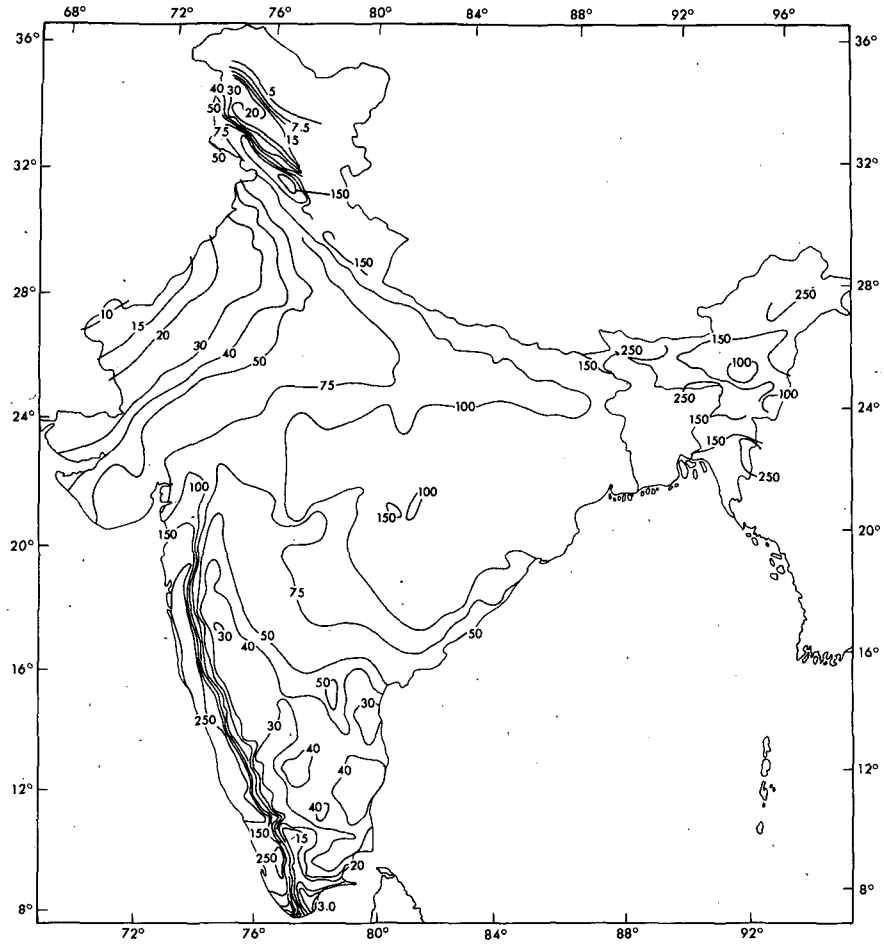

FIG. 6. Observed long-term mean precipitation over India (in cm) during June–September (from Rao, 1976).

winds, temperatures and eddy kinetic energies—along with a comparison with observations, lower resolution spectral models, and gridpoint models, can be found in Manabe *et al.* (1979).

3. Sigma-coordinates versus pressure coordinates

The model's σ-coordinate vorticity equation reads as follows:

$$\frac{\partial \zeta_\sigma}{\partial t} = -\nabla_\sigma \cdot (f + \zeta_\sigma)\mathbf{V} - \mathbf{k} \cdot (\nabla_\sigma \times RT\nabla \ln p_s) - \mathbf{k} \cdot \left(\nabla_\sigma \times \dot{\sigma} \frac{\partial \mathbf{V}}{\partial \sigma}\right) + F_\sigma. \quad (4)$$

The first term on the right can be split into horizontal advection, $-\mathbf{V} \cdot \nabla_\sigma(f + \zeta_\sigma)$, and stretching, $-(f + \zeta_\sigma)D_\sigma$. The physical significance of the second term can be made more transparent if one assumes that the flow is in approximate thermal wind balance. In σ-coordinates geostrophy, $f\mathbf{V} = \mathbf{k} \times (\nabla_\sigma \phi + RT\nabla \ln p_s)$, and hydrostatic balance, $\partial\phi/\partial\sigma = -RT/\sigma$, imply that

$$f\frac{\partial \mathbf{V}}{\partial \ln \sigma} = R\mathbf{k} \times \left(-\nabla_\sigma T + \frac{\partial T}{\partial \ln \sigma} \nabla \ln p_s\right).$$

Therefore,

$$f\frac{\partial \mathbf{V}}{\partial \ln \sigma} \cdot \nabla \ln p_s = -R\mathbf{k} \cdot (\nabla_\sigma T \times \nabla \ln p_s) = -R\mathbf{k} \cdot (\nabla_\sigma \times T\nabla \ln p_s). \quad (5)$$

From (3) we have

$$fD = fD_\sigma - f\frac{\partial \mathbf{V}}{\partial \ln \sigma} \cdot \nabla \ln p_s = fD_\sigma + \mathbf{k} \cdot (\nabla_\sigma \times RT\nabla \ln p_s) \quad (6)$$

for a flow in thermal wind balance. The plot of the model's July mean of (a) $f(D - D_\sigma)$ and (b) $\mathbf{k} \cdot (\nabla_\sigma \times RT\nabla \ln p_s)$ at $\sigma = 0.205$ in Fig. 7 show that (6) is

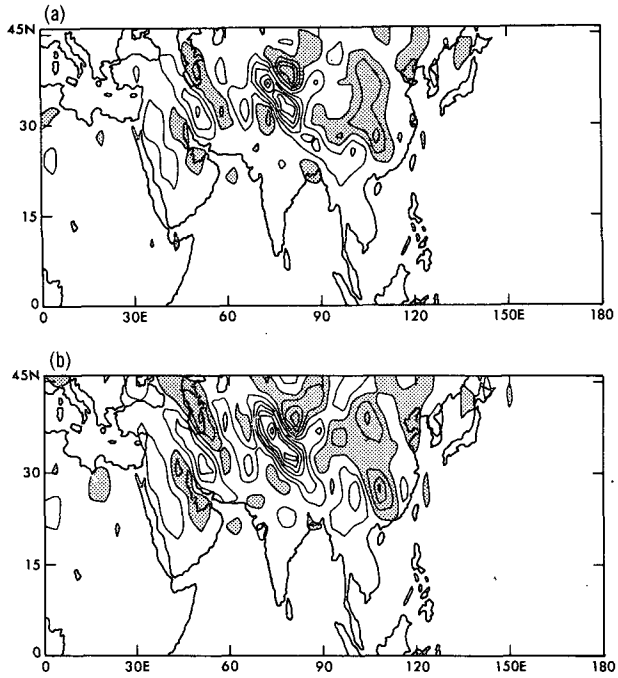

FIG. 7. July mean (a) $f(D - D_\sigma)$ and (b) $\mathbf{k}\cdot\nabla\times RT\nabla \ln p_s$ at $\sigma = 0.205$. Contour interval is 2×10^{-10} s^{-2}. The contours drawn are $\pm1, \pm3, \pm5\times10^{-10}$ s^{-2}, etc. Values less than -1×10^{-10} s^{-2} are shaded.

a rather good approximation. Therefore, one can think of the second term in (4) as a correction to σ-coordinate stretching that converts it into an estimate of the pressure coordinate stretching.

The third term in (4) accounts for vertical advection and twisting. The fourth term F_σ consists simply of a biharmonic horizontal diffusion, $-\nu\nabla_\sigma{}^4\zeta_\sigma$, with $\nu = 10^{16}$ m^4 s^{-1}. There is vertical diffusion in the model's lowest few levels, but not at the upper tropospheric levels being examined here.

The corresponding vorticity equation in pressure coordinates is

$$\frac{\partial\zeta}{\partial t} = -\nabla\cdot(f+\zeta)\mathbf{V} - \mathbf{k}\cdot\nabla\times\omega\frac{\partial\mathbf{V}}{\partial p} + F_p. \quad (7)$$

We have attempted to use the model's exact σ-vorticity balance as a starting point for obtaining a pressure coordinate balance, writing

$$\left.\begin{aligned} \frac{\partial\zeta}{\partial t} &= \frac{\partial_\sigma\zeta_\sigma}{\partial t} + R_1 \\ \nabla\cdot(f+\zeta)\mathbf{V} &= \nabla_\sigma\cdot(f+\zeta_\sigma)\mathbf{V} + R_2 \\ \mathbf{k}\cdot\nabla\times\omega\frac{\partial\mathbf{V}}{\partial p} &= \mathbf{k}\cdot\nabla_\sigma\times\dot\sigma\frac{\partial\mathbf{V}}{\partial\sigma} + R_3 \\ F_p &= F_\sigma + R_4 \end{aligned}\right\}.$$

(Note that F_p does *not* equal $-\nu\nabla^4\zeta$). Explicit expressions for R_1, R_2 and R_3 are provided in the Appendix, while one possible expression for R_4 is simply $-(R_1 + R_2 + R_3) + \mathbf{k}\cdot\nabla_\sigma\times RT\nabla \ln p_s$, since both (4) and (7) must be satisfied at any point in space. To determine whether or not an adequate pressure coordinate vorticity balance can be obtained, we set all frictional stresses in the model equal to zero (so that $F_\sigma = F_p = R_4 = 0$), computed R_1, R_2, R_3 and the pressure gradient term while integrating forward in time, and checked whether or not the equation

$$R_1 + R_2 + R_3 - \mathbf{k}\cdot\nabla_\sigma\times RT\nabla \ln p_s = 0 \quad (8)$$

was satisfied. The results were unsatisfactory. Presumably there exists a finite differenced form of the vertical derivatives in the expressions for R_1, R_2, and R_3 such that the model's exactly balanced σ-coordinate vorticity equation can be translated into an exact pressure coordinate balance, but due to the complexity of these expressions we have been unable to find such a scheme. We do find however, that the dominant terms in (8) are R_2 and the surface pressure gradient term, with R_1 and R_3 a factor of 3 or so smaller in the monsoon region. Furthermore, the dominant contribution to R_2 is simply $f(D - D_\sigma)$, which we have already seen balances $k\cdot\nabla_\sigma\times RT\nabla \ln p_s$ rather well. (The residuals we found in (8) were of the same order as R_1 and R_3 but considerably smaller than R_2). We therefore advise the reader accustomed to thinking in terms of a pressure coordinate vorticity equation to think of the following as being adequate identifications for our purposes

$$\left.\begin{aligned} (f+\zeta)D &\rightleftarrows (f+\zeta_\sigma)D_\sigma + \mathbf{k}\times(\nabla_\sigma\times RT\nabla \ln p_s) \\ \mathbf{V}\cdot\nabla(f+\zeta) &\rightleftarrows \mathbf{V}\cdot\nabla_\sigma(f+\zeta_\sigma) \\ \mathbf{k}\cdot\nabla\times\omega\frac{\partial\mathbf{V}}{\partial p} &\rightleftarrows \mathbf{k}\cdot\nabla_\sigma\times\dot\sigma\frac{\partial\mathbf{V}}{\partial\sigma} \end{aligned}\right\}. \quad (9)$$

4. The vorticity balance

Denoting a time average on the $\sigma = 0.205$ surface over the month under examination by square brackets and deviations from this mean by asterisks, one finds that $[\partial\zeta_\sigma/\partial t]$ is totally negligible in the vorticity balance, which then reduces to

$$\begin{aligned} 0 = &-\nabla_\sigma\cdot((f+[\zeta_\sigma])[\mathbf{V}] + [\zeta_\sigma^*\mathbf{V}^*]) - \mathbf{k}\cdot R\nabla_\sigma \\ &\times([T][\nabla \ln p_s] + [T^*\nabla \ln p_s^*]) - \mathbf{k}\cdot\nabla\sigma \\ &\times\left([\dot\sigma]\frac{\partial[\mathbf{V}]}{\partial\sigma} + \left[\dot\sigma^*\frac{\partial\mathbf{V}^*}{\partial\sigma}\right]\right) - \nu\nabla^4[\zeta_\sigma]. \end{aligned} \quad (10)$$

We further split the divergence of the mean vorticity flux into

$$\begin{aligned} &-\nabla_\sigma\cdot(f+[\zeta_\sigma])[\mathbf{V}] \\ &\quad = -[\mathbf{V}]\cdot\nabla_\sigma(f+[\zeta_\sigma]) - (f+[\zeta_\sigma])[D_\sigma] \end{aligned}$$

and combine the second term with the mean of the surface pressure gradient term, as discussed in Section 3, to yield what we refer to as the mean "corrected stretching"

$$-(f+[\zeta_\sigma])[D_\sigma]-\mathbf{k}\cdot R\nabla_\sigma\times[T][\nabla\ln p_s].$$

In Fig. 8 we split the vorticity budget into five terms: a) mean corrected stretching; b) mean horizontal advection, $-[\mathbf{V}]\cdot\nabla_\sigma(f+[\zeta_\sigma])$; c) mean vertical advection and twisting, $-\mathbf{k}\cdot\nabla_\sigma\times([\dot\sigma][\partial\mathbf{V}]/\partial\sigma)$; d) total transience, equal to the sum of the three terms involving starred quantities in (10); and e) diffusion, $-\nu\nabla^4[\zeta_\sigma]$. The contours in these figures correspond to $\pm1\times10^{-10}$, $\pm3\times10^{-10}$, $\pm5\times10^{-10}$ s^{-2}, etc. Inclusion of the zero contour would have resulted in even noisier plots. Values less than -1×10^{-10} s^{-2} are shaded.

As expected, the mean corrected stretching resembles the mean divergence field itself. (The surface pressure gradient correction has only a modest effect on this term, comparable to the difference between $[D]$ and $[D_\sigma]$.) The generally anticyclonic vorticity source over the continental monsoonal region is interrupted by a strong source of cyclonic vorticity south of the Himalayas, corresponding to the dry zone in Fig. 5. A clear out-of-phase relationship is evident in (a) and (b) over India and southeast Asia so that much of the stretching is balanced by horizontal advection. It is the advection of relative vorticity which is responsible for nearly all of the structure in (b), βv being small in comparison. Linearization of the relative vorticity advection,

$$-\frac{[\tilde u]}{a\cos\theta}\frac{\partial[\zeta]'}{\partial\lambda}-\frac{[v]'}{a}\frac{\partial[\zeta]}{\partial\theta},$$

where a tilde refers to a zonal average and a prime to deviations from this average, produces vorticity tendencies that bear no resemblance to those in (b).

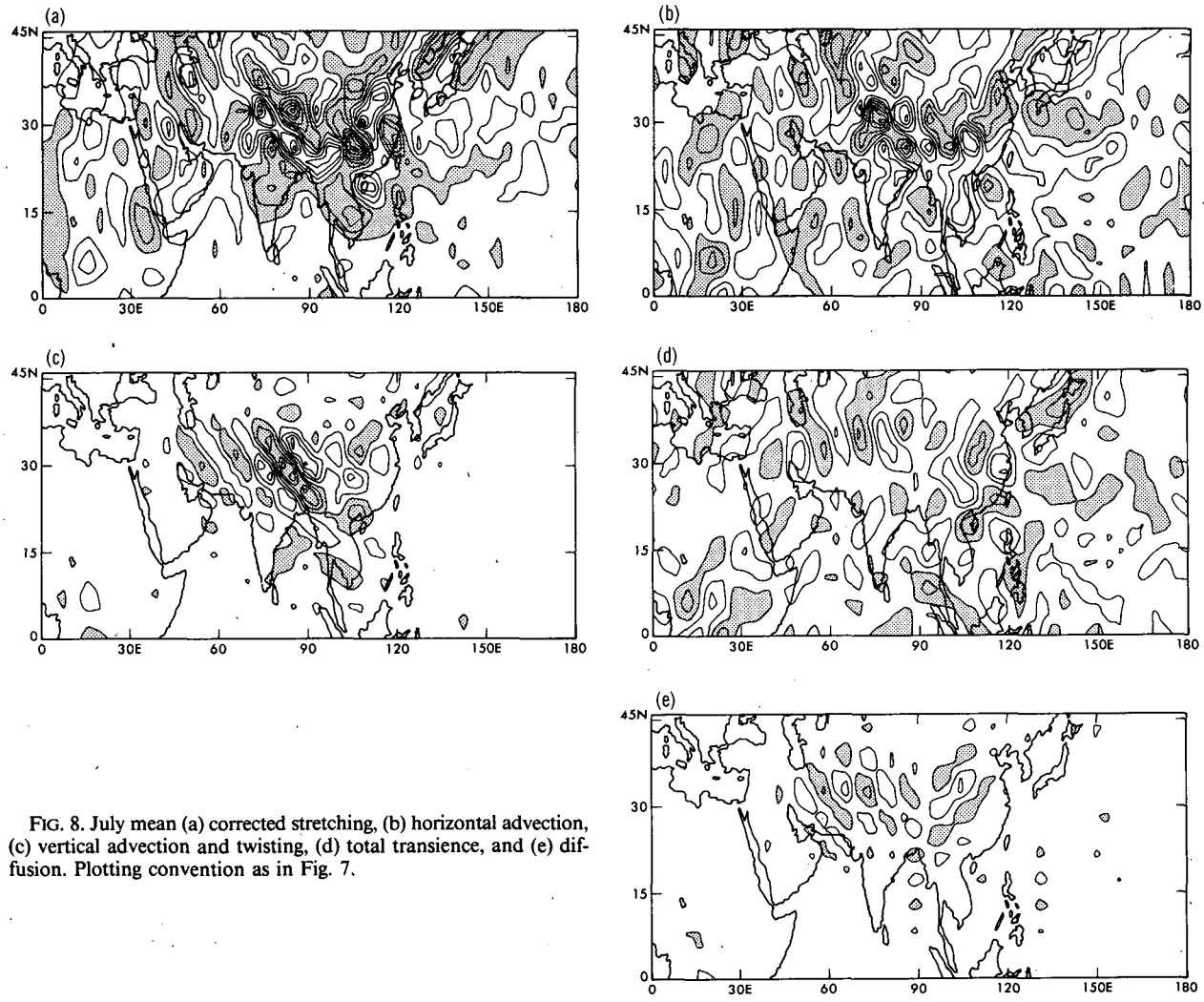

FIG. 8. July mean (a) corrected stretching, (b) horizontal advection, (c) vertical advection and twisting, (d) total transience, and (e) diffusion. Plotting convention as in Fig. 7.

Despite the cancellation between (a) and (b), their sum is still far from negligible and is balanced primarily by the mean vertical advection and twisting (c). Small horizontal scales in the mean vertical velocity field result in this term being comparable in magnitude to the stretching; (c) shows a well-defined wavetrain emanating from the Tibetan plateau. Because its wavelength is close to the limit of the model's resolution, one suspects that it is an artifact of the model numerics. This wavetrain does, however, seem to be associated with the region of upper level convergence south of the Tibetan plateau that the observed precipitation pattern suggests may correspond to a real feature. Admittedly, since the various terms in the vorticity budget have considerable structure in the smallest scales of the model, the details of the budget are likely to be unreliable.

The contribution from transients is almost entirely due to the term $-\nabla\cdot[V^*\zeta^*]$. We suspect that the pattern (d) of the transient forcing would vary substantially from one July simulation to the next; e.g., only a small number of disturbances similar to monsoon depressions form within one month in this simulation. Their effect on the vorticity budget is not negligible in certain regions. The cyclonic tendency over India and Southeast Asia, for example, is perhaps only a factor of 2 smaller than the similar tendency due to advection. However, there is much less correlation between the stretching and the transient forcing, and is not nearly as clear as the correlation with the advection. Tendencies due to horizontal diffusion (e) are even smaller. The model's budget can therefore be described as essentially nonlinear and nearly inviscid.

One is tempted to smooth the tendencies in some way so as to produce a more easily understood balance. One approach is to operate on (4) with the inverse of the Laplacian (denoted by ∇_σ^{-2}) so that the left side of (4) reduces to

$$\frac{\partial}{\partial t}\nabla_\sigma^{-2}\zeta_\sigma = \frac{\partial}{\partial t}\psi_\sigma.$$

Performing this analysis, we find the dominant terms to be

$$\frac{\partial}{\partial t}[\psi_\sigma] = 0 \approx -\nabla^{-2}(\beta[v]) - \nabla^{-2}\{(f+[\zeta_\sigma])[D_\sigma] + \mathbf{k}\cdot\nabla_\sigma\times R[T][\nabla \ln p_s]\},$$

i.e., a Sverdrup balance between the smoothed corrected stretching and the smoothed meridional advection of planetary vorticity. The two terms on the right-hand side are shown in Figs. 9(a) and (b). Note that the maximum in Fig. 9(b) off the southeast Asian coast and the zero-line over Arabia are both shifted westward compared to the corresponding features in the χ-field. Furthermore, it is potentially misleading

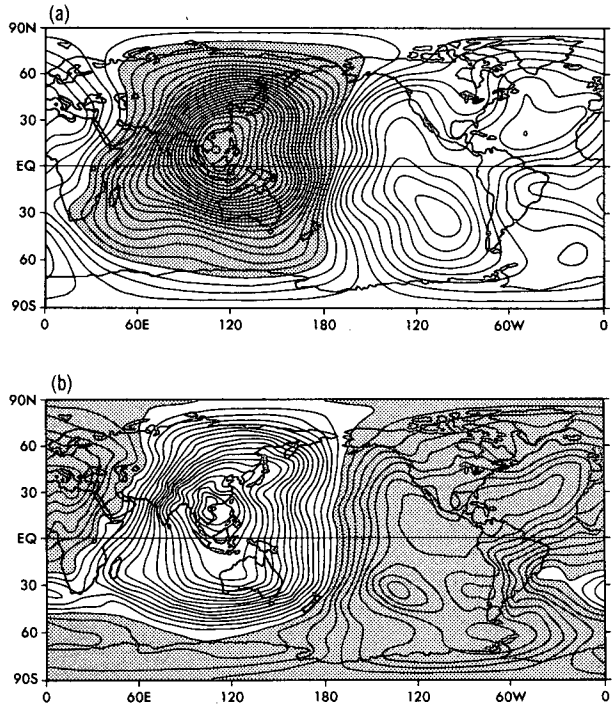

FIG. 9. July mean (a) $-\nabla^{-2}(\beta[v])$ and (b) $-\nabla^{-2}\{(f+[\zeta_\sigma])[D_\sigma] + \mathbf{k}\cdot\nabla\times R[T][\nabla \ln p_s]\}$. Contour interval is 10^{-12} s^{-2}. Negative values are shaded.

to try to infer the circulation from the term $\nabla_\sigma^{-2}(\beta[v])$ that balances this stretching. Whereas the flow is nearly zero near the streamfunction maximum over the Tibetan plateau, $\nabla_\sigma^{-2}(\beta[v])$ is large and positive there. From Fig. 9 one might guess that this anticyclone, or the zero in meridional velocity, was located at ~50°E longitude rather than at 85°E.

5. A linear model of the vorticity balance

Following Holton and Colton (1972), we consider the following steady barotropic vorticity equation on a sphere, linearized about the zonal mean wind $\tilde{u}$

$$\frac{\tilde{u}}{a\cos\theta}\frac{\partial}{\partial\lambda}\nabla^2\psi' + \frac{1}{a\cos\theta}\frac{\partial\psi'}{\partial\lambda}\left(\beta + \frac{1}{a}\frac{\partial\tilde{\zeta}}{\partial\theta}\right) = F(\lambda,\theta) - r\nabla^2\psi'. \quad (11)$$

In (11) F is a time-independent forcing function and r is a constant determining the strength of a linear vorticity damping. Holton and Colton set F equal to $-(f+\tilde{\zeta})\nabla\cdot V$ as determined by Krishnamurti at 200 mb for the summer of 1967. Using observed values of $\tilde{u}$ and $\tilde{\zeta}$ as functions of latitude, they solve for the steady state streamfunction for different values of r and find solutions resembling the observed streamfunction only for values of r corresponding to damping times r^{-1} of less than one day.

We perform a similar analysis, using the GCM output; $\tilde{u}$ and $\tilde{\zeta}$ are set equal to their simulated July mean values at $\sigma = 0.205$, and F is set equal to the July mean corrected stretching with the zonal mean removed. (It makes little difference to the solutions if the mean fields and forcing are interpolated to a constant pressure surface.) Fig. 10 shows the solution ψ' over the sphere for damping times $r^{-1} = 2$ days and 20 days. The GCM's streamfunction at $\sigma = 0.205$ with the zonal mean removed is shown in Fig. 10c for comparison. The solution for $r^{-1} = 2$ days, while far from perfect, compares much more favorably with the model's streamfunction in the Northern Hemisphere tropics than does the solution for $r^{-1} = 20$ days. The Tibetan and Mexican highs and the tilted midocean troughs are all recognizable, and the Tibetan high in particular has more or less the correct amplitude. Increasing r^{-1} destroys this agreement rather quickly; beyond a value of 5 days or so, the solution is very similar to that for 20 days, shown in Fig. 10(b), in which the amplitudes are much too large with small spurious highs and lows appearing upstream of the Tibetan and Mexican highs. Not surprisingly, the solution is particularly disastrous near 30°N where $\tilde{u}$ makes a transition from easterlies to westerlies. Note also that the GCM's eddy streamfunction is more nearly antisymmetric about the equator than the solutions to the linear model. Indeed, no linear model can simulate this nearly antisymmetric streamfunction given the asymmetry of the forcing with most of the heating and upper level divergence north of the equator.

As described in the previous section, the parameterized sub-grid scale mixing in the GCM plays a very small role in the vorticity budget. Therefore, the large damping required in (11) must be crudely accounting for terms neglected in (4), principally nonlinearity in horizontal advection, as well as vertical advection and twisting. For confirmation, we compute

$$r_{\text{eff}} \equiv -\frac{\int_S B\zeta ds}{\int_S \zeta^2 ds},$$

where B is the sum of these neglected terms and S is the area of interest. Setting S equal to the entire belt between 25°S and 45°N we find $r_{\text{eff}} \approx 1.5 \times 10^{-7}$ s^{-1}. However, r_{eff} over the monsoon region (45°E–135°E, 10°N–45°N) is considerably larger, $\approx 2 \times 10^{-6}$ s^{-1}. By confining the integration area S to a smaller region centered on the Tibetan plateau, one can raise r_{eff} to values as large as 10^{-5} s^{-1}, but the value of r_{eff} is then very sensitive to the precise location of S.

The magnitude of the stretching F over the Tibetan plateau in Fig. 8a is $\approx 1 \times 10^{-9}$ s^{-2}. If the balance in the vorticity equation is to a first approximation $V \cdot \nabla\zeta \approx F$, and if one uses the nonlinear scaling $(V \cdot \nabla) \approx \zeta$, then $\zeta \approx F^{1/2} \approx 3 \times 10^{-5}$ s^{-1}, which is the observed magnitude of the Tibetan anticyclone. To obtain reasonable results from the linear model (11) one has to choose r sufficiently large that the balance is essentially $r\zeta \approx F$ in regions of strong forcing, so that r must be of the order of $\zeta \approx 2$–3 day^{-1}.

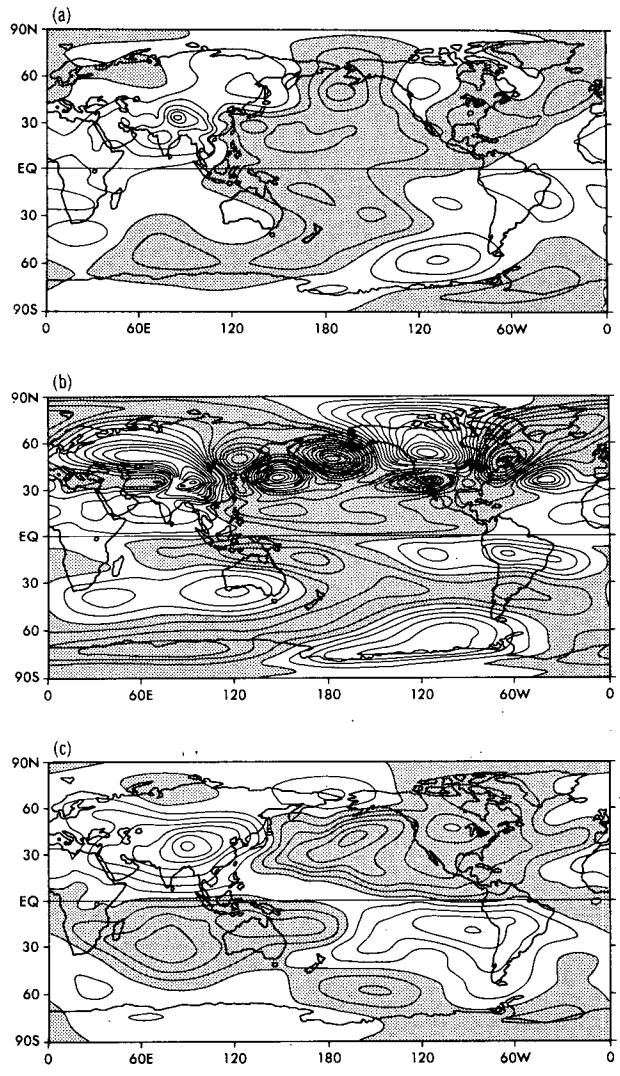

FIG. 10. Perturbation streamfunction ψ' obtained for damping time (a) 2 days, and (b) 20 days. The GCM's July mean ψ' is shown in (c). Contour interval is 5×10^6 m^2 s^{-1}. Negative values are shaded.

6. Summary

Our analysis of the time-mean vorticity balance in a high resolution spectral GCM constructed at GFDL yields the following results.

- The model produces what we believe is a reasonable simulation of the large scale features of the Northern summer 200 mb flow in the tropics without the

inclusion of sub-grid scale processes that strongly damp the upper tropospheric vorticity. There is considerable cancellation between the stretching and horizontal advection of vorticity in the vicinity of the Tibetan anticyclone with most of the remainder balanced by vertical advection and twisting. Much of the structure in these terms occurs on scales close to the limit of the model's resolution. While the spatial separation between the model's streamfunction and velocity potential maxima is much larger than in Krishnamurti's analysis of 1967, it is comparable to that in the ECMWF analysis of 1979. As pointed out by a reviewer, 1967 was a year with a strong monsoon over India and 1979 a year with a weak monsoon; however, the model monsoon produces ample rainfall over India (Fig. 5). In any case, in the absence of a satisfactory vorticity budget for the observed flow, it seems reasonable to assume that the basic character of the budget does not change from year to year.

⊙ Transients in the model play only a minor role in the vorticity budget; what effect there is arises from the divergence of the horizontal vorticity flux. Subgrid scale mixing is of even less importance.

⊙ The dominant balance of the streamfunction tendency equation is between the inverse Laplacian of the stretching (closely resembling the velocity potential) and the inverse Laplacian of βv. However, it is difficult to infer v itself, or the mean position of the model's Tibetan Anticyclone, from a plot of $\nabla^{-2}(\beta v)$.

⊙ A calculation identical to that of Holton and Colton with the linearized barotropic vorticity equation, using the model's zonal mean flow and mean divergence forcing, results in a rough approximation to the model's Tibetan anticyclone only with very large values of the damping coefficient. This damping is found to crudely account primarily for nonlinearity in the horizontal advection.

These results do not prove that a cumulus-scale momentum transport is of little importance for the time-mean monsoonal flow. Some mixing of momentum in regions of intense convection could very well smooth out some of the smaller scale features in the vorticity field, decreasing the importance of nonlinearity in the horizontal advection for the vorticity budget. It is possible that the model's tropical vorticity budget is different from that of the real atmosphere, particularly since the terms in the budget have considerable structure on the smallest scales that can be resolved by the GCM.

Acknowledgments. We would like to thank S. Manabe, D. Hahn, and L. Holloway for advice and assistance with the general circulation model, and the Scientific Illustration Group at GFDL for drawing the detailed figures. One of the authors (PDS) was supported by NOAA Grant 04-7-022-44017 and NSF Grant ATM-7719955.

APPENDIX

Expressions for R_1, R_2, and R_3

Expressions for R_1, R_2, and R_3 are given as follows:

$$\left.\begin{aligned} R_1 &= \frac{\partial R_\zeta(\mathbf{V})}{\partial t} - \frac{\partial}{\partial \ln\sigma}(\zeta_\sigma + R_\zeta(\mathbf{V}))\left(\frac{\partial \ln p_s}{\partial t}\right) \\ R_2 &= \nabla_\sigma \cdot (R_\zeta(\mathbf{V})\mathbf{V}) + R_D((\zeta_\sigma + R_\zeta(\mathbf{V}) + f)\mathbf{V}) \\ R_3 &= \mathbf{k}\cdot\nabla_\sigma \times \sigma \frac{d \ln p_s}{dt}\frac{\partial \mathbf{V}}{\partial \sigma} \\ &\quad + R_\zeta\left(\dot{\sigma}\frac{\partial \mathbf{V}}{\partial \sigma} + \sigma \frac{d \ln p_s}{dt}\frac{\partial \mathbf{V}}{\partial \sigma}\right) \end{aligned}\right\},$$

where for any vector $\mathbb{L}$,

$$\left.\begin{aligned} R_\zeta(\mathbb{L}) &= \mathbb{k}\cdot\frac{\partial \mathbb{L}}{\partial \ln\sigma} \times \nabla \ln p_s \\ R_D(\mathbb{L}) &= -\frac{\partial \mathbb{L}}{\partial \ln\sigma}\cdot\nabla \ln p_s \end{aligned}\right\}.$$

REFERENCES

Abbott, D. A., 1977: Hemispheric simulation of the Asian summer monsoon. *Pure Appl. Geophys.*, **115**, 1111–1130.

Bengtsson, L., M. Kanamitsu, P. Källberg and S. Uppala, 1982: FGGE research activities at ECMWF. *Bull. Amer. Meteor. Soc.*, **71**, 277–303.

Chang, C.-P., 1977a: Viscous internal gravity waves and low frequency oscillations in the tropics. *J. Atmos. Sci.*, **34**, 901–910.

——, 1977b: Some theoretical problems of the planetary scale monsoons. *Pure Appl. Geophys.*, **115**, 1087–1109.

Chu, J.-H., M. Yanai and C.-H. Sui, 1981: Effects of cumulus convection on the vorticity field in the tropics. Part I: The large scale budget. *J. Meteor. Soc. Japan*, **59**, 535–546.

Colton, D. E., 1973: Barotropic scale interactions in the tropical upper troposphere during the northern summer. *J. Atmos. Sci.*, **30**, 1287–1302.

Fein, J. S., 1977: Global vorticity budget over the tropics and subtropics at 200 mb during the Northern Hemisphere summer. *Pure Appl. Geophys.*, **115**, 1493–1500.

Gill, A. F., 1980: Some simple solutions for heat-induced tropical circulation. *Quart. J. Roy. Meteor. Soc.*, **106**, 447–462.

Hodur, R. M., and J. S. Fein, 1977: A vorticity budget over the Marshall Islands during the spring and summer months. *Mon. Wea. Rev.*, **105**, 1521–1526.

Holton, J. R., and D. E. Colton, 1972: A diagnostic study of the vorticity balance at 200 mb in the tropics during the northern summer. *J. Atmos. Sci.*, **29**, 1124–1128.

Kanamitsu, M., 1977: Monsoonal quasi-stationary ultra long waves of the tropical troposphere predicted by a real data prediction over a global tropical belt. *Pure Appl. Geophys.*, **115**, 1187–1208.

Krishnamurti, T. N., 1971a: Observational study of the tropical upper troposphere motion field during the Northern Hemisphere summer. *J. Appl. Meteor.*, **10**, 1066–1096.

——, 1971b: Tropical east–west circulations during the northern summer. *J. Atmos. Sci.*, **28**, 1342–1347.

Manabe, S., 1969: Climate and ocean circulation, Part I. The atmospheric circulation and hydrology of the earth's surface. *Mon. Wea. Rev.*, **97**, 739–774.

——, J. Smagorinsky and R. F. Strickler, 1965: Simulated climatology of a general circulation model with a hydrological cycle. *Mon. Wea. Rev.*, **93,** 769–798.

——, D. G. Hahn and J. L. Holloway, Jr., 1979: Climate simulations with GFDL spectral models of the atmosphere: Effect of spectral truncation. *Rep. JOC Study Conference on Climate Models: Performance, Intercomparison and Sensitivity Studies,* Washington, DC, GARP Publ. Ser. No. 22, Vol. 1, 41–94 [NTIS N8027917].

Rao, Y. P., 1976: *Southwest Monsoon. Meteor. Monogr.,* No. 1, Indian Meteor. Dept., 367 pp.

Reed, R. J., and R. H. Johnson, 1974: The vorticity budget of synoptic-scale wave disturbances in the tropical western Pacific. *J. Atmos. Sci.,* **31,** 1784–1790.

Reeves, R. W., C. F. Ropelewski and M. D. Hudlow, 1979: Relationship between large-scale motion and convective precipitation during GATE. *Mon. Wea. Rev.*, **107,** 1154–1168.

Sardeshmukh, P. D., 1982: Mechanisms of monsoonal cyclogenesis. Ph.D. thesis, Princeton University, Princeton, NJ.

Shapiro, L. J., 1978: The vorticity budget of a composite African tropical wave disturbance. *Mon. Wea. Rev.*, **106,** 806–817.

Stevens, D. E., 1979: Vorticity, momentum and divergence budgets of synoptic-scale wave disturbances in the tropical Atlantic. *Mon. Wea. Rev.*, **107,** 535–550.

Williams, K. T., and W. M. Gray, 1973: Statistical analysis of satellite observed trade wind cloud clusters in the western North Pacific. *Tellus,* **25,** 313–336.